Engineering 3 (2017) 285–289

Contents lists available at ScienceDirect

Engineering

journal homepage: www.elsevier.com/locate/eng

Research
Green Chemical Engineering—Letter

Improved Oxygen Evolution Kinetics and Surface States Passivation of Ni-B_i Co-Catalyst for a Hematite Photoanode

Ke Dang [a,b], Tuo Wang [a,b], Chengcheng Li [a,b], Jijie Zhang [a,b], Shanshan Liu [a,b], Jinlong Gong [a,b,*]

[a] *Key Laboratory for Green Chemical Technology of Ministry of Education, School of Chemical Engineering and Technology, Tianjin University, Tianjin 300072, China*
[b] *Collaborative Innovation Center of Chemical Science and Engineering, Tianjin 300072, China*

ARTICLE INFO

Article history:
Received 19 January 2017
Revised 18 March 2017
Accepted 22 March 2017
Available online 17 May 2017

Keywords:
Nickel-borate
Hematite
Oxygen evolution reaction
Co-catalyst

ABSTRACT

This paper describes the combinational surface kinetics enhancement and surface states passivation of nickel-borate (Ni-B_i) co-catalyst for a hematite (Fe_2O_3) photoanode. The Ni-B_i-modified Fe_2O_3 photoanode exhibits a cathodic onset potential shift of 230 mV and a 2.3-fold enhancement of the photocurrent at 1.23 V, versus the reversible hydrogen electrode (RHE). The borate (B_i) in the Ni-B_i film promotes the release of protons for the oxygen evolution reaction (OER).

1. Introduction

Since Fujishima and Honda's seminal report on photoelectrochemical (PEC) hydrogen evolution [1], extensive research has been devoted toward various semiconductors that are capable of meeting the strict requirements for solar-to-fuel devices. Despite theoretically high efficiencies, most electrodes based on oxide semiconductors suffer from rapid charge recombination on the surface and/or in the bulk. Hematite (Fe_2O_3), with a suitable bandgap of 2 eV, for example, has low charge-separation efficiency and slow oxygen evolution kinetics.

To overcome such challenges, oxygen evolution catalysts (OECs) have often been coupled with oxide semiconductors to catalyze water oxidation [2], which is considered to be the rate-limiting step for both PEC water splitting and CO_2 reduction. In addition to the high-cost platinum group metal oxides, earth-abundant OECs (e.g., metal oxides and hydroxides) [3] have been investigated as a way to accelerate the surface reaction kinetics of semiconductors. In particular, cobalt-phosphate (Co-P_i) complexes have been demonstrated to enhance the oxygen evolution reaction (OER) performance of oxide semiconductors such as Fe_2O_3 [4] and WO_3 [5]. Nickel-borate (Ni-B_i) has also been demonstrated by Dincă et al. [6] to have electrochemical catalytic properties that are similar to those of Co-P_i. The formula of Ni-B_i has been suggested to be $NiO(OH)_{2/3}(H_2BO_3)_{1/3}\cdot 1.5H_2O$ by elemental analysis [6]. A further dramatic increase in catalytic performance can be achieved by anodic activation of the electrodeposited Ni-B_i films [7]. It has been shown that the efficiency of proton and electron transfer for Ni-B_i OEC is the same as for IrO_x, and higher than for $Ni(OH)_2$ [6]. Thus, Ni-B_i is a very promising OEC for photoanodes. Ni-B_i has been demonstrated to successfully catalyze OER over a $BiVO_4$ photoanode, for which the photocurrent at 1.23 V versus the reversible hydrogen electrode (vs. RHE) is enhanced by a factor of 3.8 [8]. Gan et al. [9] reported that the loading of Ni-B_i on a $BiVO_4$ photoanode enables a 350 mV cathodic shift of onset potential for oxygen evolution at pH 9. However, the role of Ni-B_i as a co-catalyst is not yet fully understood in PEC applications.

This paper describes the coupling of Ni-B_i OEC with an Fe_2O_3 photoanode for solar oxygen evolution. By comparing the OER kinetics and electrode/electrolyte interface of Ni-B_i/Fe_2O_3 with those of bare Fe_2O_3, it is demonstrated that Ni-B_i is a dual-function co-catalyst that improves oxygen evolution kinetics and realizes surface states passivation simultaneously for an Fe_2O_3 photoanode. The specific

---

* Corresponding author.
E-mail address: jlgong@tju.edu.cn

http://dx.doi.org/10.1016/J.ENG.2017.03.005

role of B_i in Ni-B_i is further explored by comparing the catalytic performance of Ni-B_i and NiOOH using solutions with different proton concentrations.

2. Results and discussion

Nanostructured Fe_2O_3 photoanodes were synthesized via a hydrothermal approach [10], and the loading of the Ni-B_i co-catalyst was carried out using a modified electrodeposition technique [6] (experimental section is provided in Supplementary Information). The obtained Fe_2O_3 shows a one-dimensional nanorod structure in the field-emission scanning electron microscopy (SEM) image (Fig. 1(a)). The film thickness is 310 ± 76 nm (see Fig. S1 in Supplementary Information). The Ni-B_i-modified photoanode shows a similar nanorod feature with a slightly smoother surface (Fig. 1(b)). The existence of the Ni-B_i layer was verified by transmission electron microscopy (TEM) and high-resolution TEM (HRTEM) images of Ni-B_i/Fe_2O_3 (Figs. 1(c) and (d)). The Fe_2O_3 in the HRTEM image displays high crystallinity with a lattice spacing of 0.27 nm (Fig. 1(d)) corresponding to the (104) plane of crystallized Fe_2O_3. The selected area electron diffraction (SAED) pattern (Fig. 1(d) inset) shows the polycrystalline structure of the Fe_2O_3 nanorod. The Ni-B_i amorphous layer is relatively uniform, with a thickness of approximately 10 nm. The absence of additional X-ray diffraction patterns upon the loading of Ni-B_i (see Fig. S2 in Supplementary Information) also suggests the amorphous nature of Ni-B_i, which is consistent with previous research [6]. It is clear from the electron energy-loss spectroscopy mapping of the nanorod (see Fig. S3 in Supplementary Information) that the bulk of each nanorod is enriched with iron (Fe), while the outer layer is rich in nickel (Ni) and boron (B). X-ray photoelectron spectroscopy (XPS) characterizations (see Fig. S4 in Supplementary Information) also corroborate the Ni-B_i overlayer on the Fe_2O_3. The ratio of Ni to B was determined to be about 1:2 by employing inductively coupled plasma mass spectrometry after dissolving the entire film of Ni-B_i/Fe_2O_3. The ultraviolet (UV)/visible light-absorbance spectra (see Fig. S5 in Supplementary Information) indicate that the Ni-B_i overlayer has a negligible influence on the light absorption of the Fe_2O_3 photoanode.

With optimized Ni-B_i loading (see Fig. S6 in Supplementary Information), photocurrent density versus applied potential (J-V) measurements were performed for Fe_2O_3 and Ni-B_i/Fe_2O_3 photoanodes (Fig. 2(a)). The bare Fe_2O_3 photoanode exhibits the typical response of a hydrothermal-prepared Fe_2O_3 electrode, with a photocurrent onset potential of 0.85 V vs. RHE, and a photocurrent of 0.48 mA·cm^{-2} at 1.23 V vs. RHE. Upon the loading of Ni-B_i, the onset of the photocurrent significantly shifts cathodically by 230 mV to 0.62 V vs. RHE. The cathodic onset potential of 0.62 V (vs. RHE) enables the use of Ni-B_i/Fe_2O_3 to construct overall water-splitting devices with suitable photocathodes, such as Cu_2O-based photocathodes (onset potential of 1.02 V vs. RHE) [11], $CuBi_2O_4$-based photocathodes (onset potential of ~1.0 V vs. RHE) [12], and Cu(In, Ga)Se-based photocathodes (onset potential of 0.65 V vs. RHE) [13]. In addition, the photocurrent increases substantially from 0.48 mA·cm^{-2} to 1.12 mA·cm^{-2} at 1.23 V vs. RHE. This performance is comparable to that of some of the best Fe_2O_3 photoanodes with OECs [10,14–16]. The improved incident-photo-to-current efficiency (IPCE) of Ni-B_i/Fe_2O_3 (Fig. 2(b)) is also consistent with the photocurrent. The applied-bias photo-to-current conversion efficiency (APCE) of the Ni-B_i/Fe_2O_3 photoanode is 0.16% at 0.97 V vs. RHE, which is 5.3 times greater than that of the bare Fe_2O_3 photoanode (0.03% at 1.03 V vs. RHE) (see Fig. S7 in Supplementary Information). Although an anodic activation process is necessary after the loading of Ni-B_i to enhance its activity (see experimental section in Supplementary Information), photocurrent enhancement due to the anodization of Fe_2O_3 itself was ruled out (see Fig. S8 in Supplementary Information). The Ni-B_i reduced the photogenerated holes that had accumulated on the Fe_2O_3 surface, as illustrated by the reduced transient spikes in the transient photocurrent measurements at 1.23 V vs. RHE under chopped illumination (see Fig. S9 in Supplementary Information). The stability of the Fe_2O_3 electrode was almost unchanged after the loading of the Ni-B_i co-catalyst (see Fig. S10 in Supplementary Information).

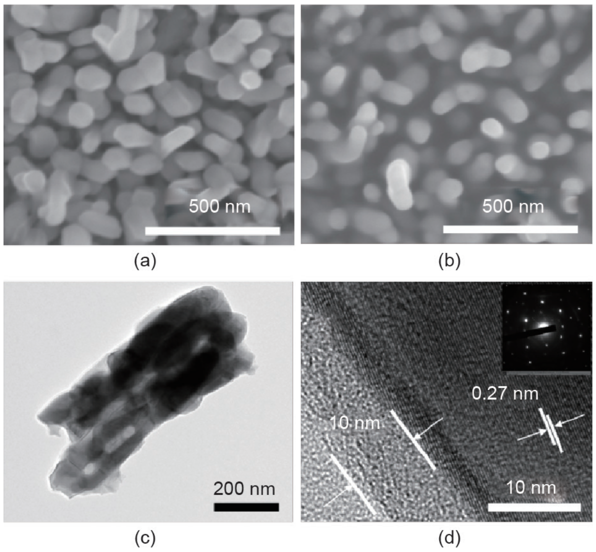

Fig. 1. SEM images of (a) Fe_2O_3 and (b) Ni-B_i/Fe_2O_3. TEM images of a Ni-B_i/Fe_2O_3 photoanode at (c) low and (d) high resolution. The inset of (d) is the SAED pattern of Ni-B_i/Fe_2O_3.

Electrochemical impedance spectroscopy (EIS) in Nyquist plots under conditions of darkness and illumination (Fig. 2(c) and (d), respectively) were obtained to further explore the enhancing mechanism of the Ni-B_i film. Fig. 2(c) indicates that the residual double-layer charge transfer resistance under darkness, which is characterized by the semidiameter of the semicircle, decreased significantly for Fe_2O_3 upon the deposition of the Ni-B_i overlayer, suggesting improved charge transfer across the electrode/electrolyte interface. Two clear semicircles are visible in Fig. 2(d) for the Fe_2O_3 and Ni-B_i/Fe_2O_3 photoanodes under illumination, indicating the existence of two capacitances [17]. A typical equivalent circuit model was used to fit the EIS data (Fig. 2(d) inset). The fitting results (see Table S1 in Supplementary Information) suggest that the series resistance (R_s) is almost unchanged after modification with Ni-B_i, which is reasonable because the interface between Fe_2O_3 and fluorine-doped tin oxide (FTO) is unchanged. A significant decrease in the charge transfer resistance at the electrode/electrolyte interface (R_{ct}) from 321.3 Ω to 166.9 Ω demonstrates that the photogenerated holes transfer into the electrolyte more easily than those on the bare Fe_2O_3 surface, due to the enhanced OER kinetics with Ni-B_i. This finding aligns with the EIS analysis under darkness. The enhanced OER kinetics with Ni-B_i is also evidenced by the Tafel slope (see Fig. S11 in Supplementary Information). The Tafel slope of the Ni-B_i/Fe_2O_3 electrode (~46 mV·decade^{-1}) is much smaller than that of the bare Fe_2O_3 electrode (~138 mV·decade^{-1}). The charge transfer resistance in the bulk electrode (R_{trap}) drops significantly, from 128.1 Ω to 90.2 Ω, upon the loading of the Ni-B_i catalyst. The R_{trap} is relevant to the charge mobility in Fe_2O_3 (conductivity) and to the lifetime of the electron/hole (charge separation). Since the conductivity of the bulk Fe_2O_3 could not change upon catalyst loading, the enhanced charge transfer may be due to improved charge separation, suggesting that Ni-B_i may play another role in addition to its surface catalytic effect. This result led us to further explore the combined effects of the Ni-B_i co-catalyst on the PEC performance.

With regard to Fe_2O_3, the surface states and the pinning effects of

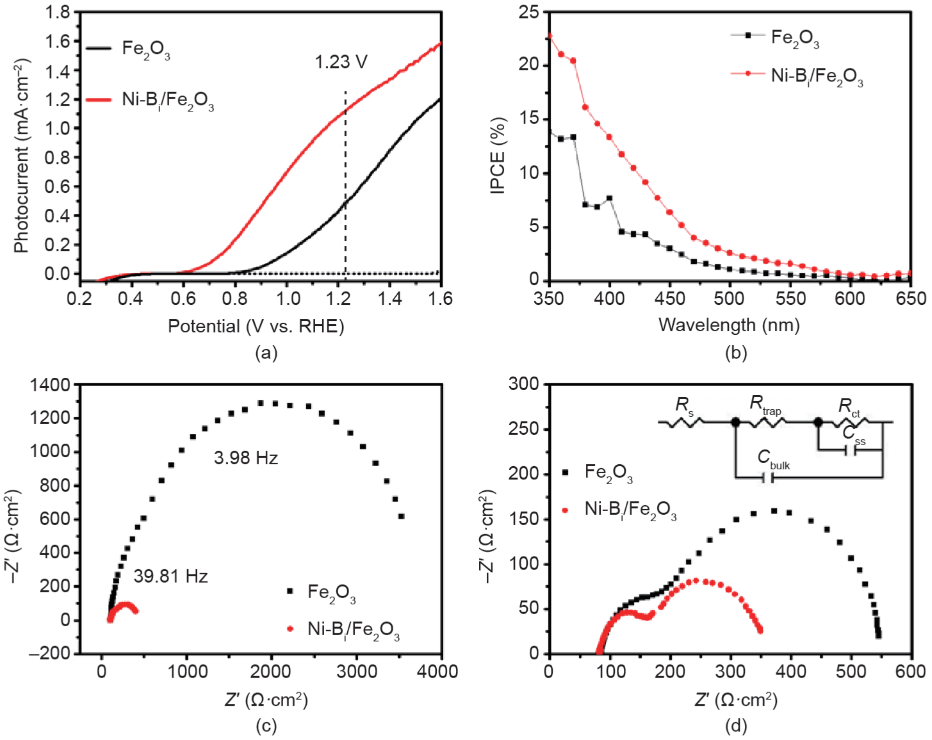

Fig. 2. (a) J-V curves recorded under air mass 1.5 global (AM 1.5G) illumination. (b) IPCE measured at 1.23 V vs. RHE. EIS in Nyquist plots measured at 1.5 V vs. RHE under (c) darkness and (d) illumination. 0.5 mol·L^{-1} KB_i electrolyte (pH 9.2) is used, as in all measurements. The electrolyte is not stirred. The inset of (d) shows the equivalent circuit of the photoanode.

the Fermi level have been investigated theoretically and experimentally [18,19]. In addition to passivation layers of, for example, Al_2O_3 [20], Du et al. have demonstrated that a surface catalytic $NiFeO_x$ layer can passivate surface states and minimize or eliminate the potential drop within the Helmholtz layer, resulting in a much higher photovoltage [21]. A higher photovoltage suggests an improvement in the thermodynamics of the system upon catalyst loading. Thus, the cathodic shift of the onset potential of an Fe_2O_3 electrode may be attributed to two aspects: kinetics and thermodynamics.

In order to identify the thermodynamics-enhancing effects of Ni-B_i, the steady-state open-circuit potential (OCP) was measured with and without illumination (Fig. 3(a)) to minimize the influence of kinetics factors. The difference in OCPs of the bare Fe_2O_3 electrode under darkness and illumination indicates a photovoltage of 0.21 V. A large photovoltage of 0.72 V is obtained upon the loading of the Ni-B_i catalyst, due to the significantly more positive OCP in the dark. The OCP in the dark usually reflects the extent of upward band bending of the photoanode in equilibrium with the electrolyte. The significantly more positive OCP (1.45 V vs. RHE) that was obtained with Ni-B_i in the dark suggests a more pronounced upward band bending, which is likely due to the fact that the surface states of Fe_2O_3 are passivated to unpin the Fermi level. Therefore, the improved photovoltage of Ni-B_i/Fe_2O_3 compared with Fe_2O_3 could be attributed to passivation of the surface states. In addition, compared with the bare Fe_2O_3 sample, the Ni-B_i-loaded sample exhibits a shift in the cathodic direction of 80 mV of effective flat-band potential (E_{FB}), as indicated by the Mott-Schottky plots of Fe_2O_3 and Ni-B_i/Fe_2O_3 (Fig. 3(b)). This cathodic shift also indicates a more pronounced band bending upon the loading of Ni-B_i, due to the passivation of surface states by the Ni-B_i overlayer that alleviates the Fermi-level pinning [15]. The photo-oxidation of an H_2O_2 scavenger was further studied (see Fig. S12 in Supplementary Information). The comparable onset potential of dark currents of Fe_2O_3 and Ni-B_i/Fe_2O_3 (see Fig. S12(a) in Supplementary Information) suggests equally fast H_2O_2 oxidation kinetics on the surface of Fe_2O_3 and Ni-B_i, where the surface catalytic effect of Ni-B_i can be excluded. It has been demonstrated that the photocurrent onset potential for a sacrificial agent with fast oxidation kinetics should be very close to E_{FB} [22]. Thus, the cathodic shift of the photocurrent onset of H_2O_2 oxidation (see Fig. S12(b) in Supplementary Information), which is consistent with our E_{FB} results, can be attributed to the enhanced thermodynamics factors owing to the passivated surface upon the loading of Ni-B_i [23,24]. The slight increase of the photocurrent (see Fig. S12(b) in Supplementary Information) is the result of reduced charge transfer resistance in the bulk electrode, which is consistent with the reduced R_{trap} from EIS.

To further verify the surface states passivation of the Ni-B_i layer, Photoluminescence (PL) tests were conducted. Whereas the recombination between the valance band and the conduction band is radiative, the recombination at the surface state is non-radiative [25]. Since the numbers of photogenerated electrons and holes are the same in the Fe_2O_3 photoanode under the same light stimulation, an increase in PL intensity, which indicates increased recombination between the valence and the conduction bands, may be the result of passivated surface states, as reported previously [26,27]. Thus, the strengthened PL intensity of Ni-B_i/Fe_2O_3 compared with Fe_2O_3 (Fig. 3(c)) suggests that the Ni-B_i layer is able to passivate the surface states of Fe_2O_3.

The specific role of B_i in Ni-B_i was also investigated. In the process of water oxidation via a Ni-B_i co-catalyst, it has been suggested that $Ni^{2+}/Ni^{3+}/Ni^{4+}$ are the active sites for oxygen evolution from water [27]. Ye et al. demonstrated that in NiOOH for a $BiVO_4$ photoanode, $Ni^{2+}/Ni^{3+}/Ni^{4+}$ are the active sites for hole transfer from $BiVO_4$ to the electrolyte and water oxidation [28]. Our XPS results (see Fig. S4(b) in Supplementary Information) also reveal the existence of Ni^{2+}/Ni^{3+} states in our Ni-B_i OEC. Thus, we propose that Ni^{2+}/Ni^{3+} sites are the main active sites for water oxidation in Ni-B_i. On the other hand, Trześniewski et al. [29] demonstrated the importance of the deprotonation of NiOOH for OER. Because B_i is a proton-accepting electrolyte, it is speculated that the B_i may facilitate the release of protons from water, and thus enhance OER in this study.

To verify this assumption, we compared the influence of protons on our Ni-based co-catalysts, with and without B_i (Ni-B_i and NiOOH), in different proton concentrations. NiOOH was loaded on a freshly prepared Fe_2O_3 electrode using a photo-assistant electrodeposition method [17]. To obtain different proton concentrations, we prepared 0.1 mol·L^{-1} KB_i aqueous electrolytes buffered to different pHs (pH 8–12), in which the overpotentials for OER on Ni-B_i/Fe_2O_3, NiOOH/Fe_2O_3, and bare Fe_2O_3 electrodes were measured (Fig. 3(d)). A higher pH of the electrolyte reflects a lower proton concentration, which is favorable to promote the release of protons from water molecules. It is generally considered that the OER in an alkaline solution is the oxidation of OH^- after the release of a proton from a water molecule [30,31]. Thus, a decreasing overpotential of OER was obtained for Fe_2O_3 and NiOOH/Fe_2O_3 electrodes with higher pH (Fig. 3(d)). In comparison, Ni-B_i/Fe_2O_3 exhibits much lower overpotentials for water oxidation over the entire tested pH range, which is owing to the catalytic effect of Ni-B_i. More importantly, the linear decreasing dependency on pH is absent in the case of Ni-B_i; in this case, the electrolytes with lower pH (i.e., higher proton concentrations) also exhibit lower overpotentials. Although the release of protons tends to occur less in electrolytes with higher proton concentrations, B_i would facilitate the release of protons from water molecules in the electrolyte [8]. It has also been demonstrated in Dincă's work that Ni-B_i loses one electron accompanied by the transfer of ~1.5 protons, compared with the one-electron-one-proton oxidation of water for NiOOH in neutral electrolyte [6]. Since the morphology of NiOOH and of Ni-B_i are almost the same (see Fig. S13 in Supplementary Information) [17], a different overpotential for the OER caused by a different surface area can be ruled out. Thus, the B_i favors the release of protons for oxygen evolution in electrolytes with high proton concentration. In addition, when the pH is higher than 9–9.5, the oxidation overpotentials of Ni-B_i/Fe_2O_3 decrease again. This phenomenon could be attributed to the limited performance of B_i for proton release. In neutral electrolytes, the OER mechanism has been suggested to be a proton-coupled electron-transfer process [32], or a direct oxidation of water molecules followed by the release of protons [33]. In these cases, B_i would also be able to promote the transfer of protons for improved OER kinetics.

Fig. 4 illustrates the kinetics and thermodynamics dual function of a Ni-B_i co-catalyst. In a bare Fe_2O_3 electrode, a hole may be trapped in surface states and then slowly recombine with an elec-

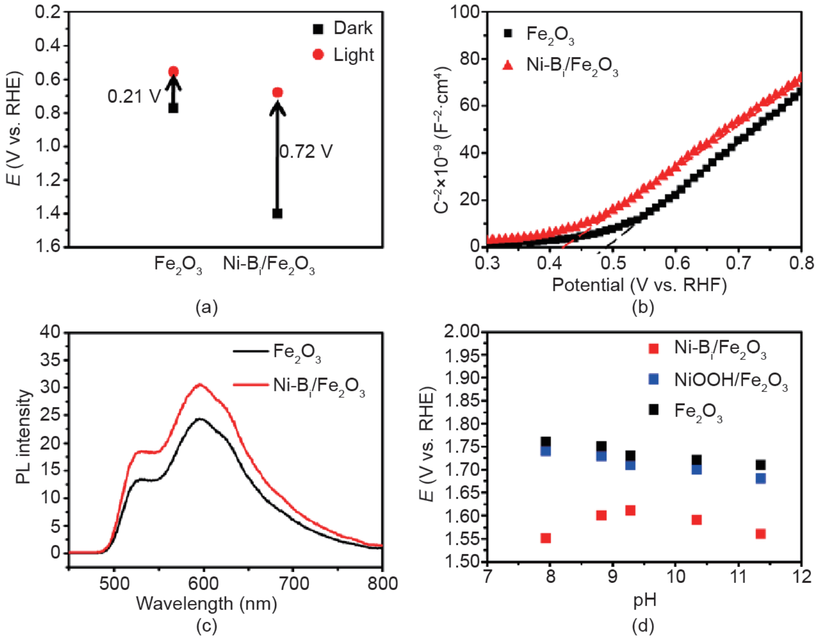

Fig. 3. (a) OCP under darkness and AM 1.5G illumination, and (b) Mott-Schottky plots recorded under darkness in 0.5 mol·L^{-1} KB_i (pH 9.2) electrolyte. (c) PL spectra of bare Fe_2O_3 and Fe_2O_3 decorated with Ni-B_i. (d) The overpotential of the water oxidation of Ni-B_i/Fe_2O_3, NiOOH/Fe_2O_3, and bare Fe_2O_3 electrode in 0.1 mol·L^{-1} KB_i buffer electrolyte at different pHs (with 2 mol·L^{-1} KNO_3 as the support electrolyte).

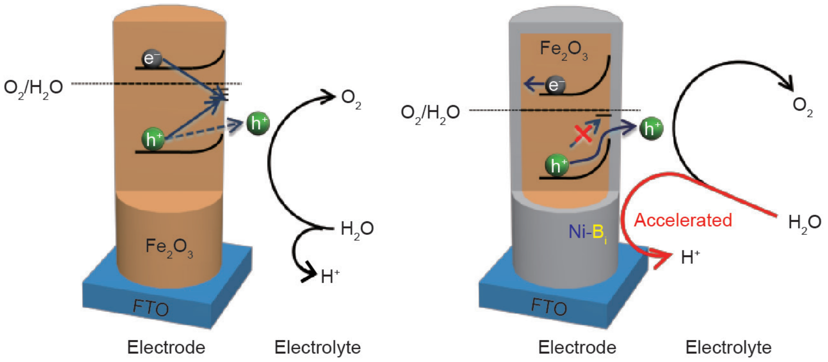

Fig. 4. Schematic illustration of the combinational effects of Ni-B_i OEC on an Fe_2O_3 photoanode.

tron instead of oxidizing water. The surface state pins the Fermi level and results in lowered band bending. In Ni-B_i-decorated Fe_2O_3, the enhanced water oxidation can be attributed to both kinetics and thermodynamics factors. The surface states passivation via Ni-B_i leads to the unpinning of the Fermi level and to a more profound upward band bending, improving the charge separation in Fe_2O_3. In addition to surface states passivation, Ni-B_i kinetically promotes OER. The B_i in the Ni-B_i is proven to promote the release of protons, thus enhancing OER on a Ni-B_i/Fe_2O_3 photoanode.

3. Conclusion

In summary, we have demonstrated that Ni-B_i co-catalyst can be coupled with an Fe_2O_3 photoanode to enhance oxygen evolution. Upon the loading of Ni-B_i, the onset of the photocurrent shifts cathodically by 230 mV to 0.62 V vs. RHE, and the photocurrent increases from 0.48 $mA \cdot cm^{-2}$ to 1.12 $mA \cdot cm^{-2}$ at 1.23 V vs. RHE. The role of Ni-B_i can be attributed to two aspects: kinetics and thermodynamics. The enhanced OER kinetics are evidenced by the significant drop of charge transfer resistance at the electrode/electrolyte interface, as well as by the decreased Tafel slope upon the loading of Ni-B_i. The passivation of surface states is verified by a much larger photovoltage and by the cathodic shift of the effective flat-band potential, which is due to a more pronounced upward band bending with alleviated Fermi-level pinning. PL intensity also reveals the passivation of surface states. In the process of water oxidation, the B_i in the Ni-B_i film promotes the release of protons from water molecules to improve OER.

Acknowledgements

We acknowledge the National Key Research and Development Program of China (2016YFB0600901), the National Natural Science Foundation of China (21525626, U1463205, U1662111), the Specialized Research Fund for the Doctoral Program of Higher Education (20130032120018), and the Program of Introducing Talents of Discipline to Universities (B06006) for financial support.

Compliance with ethics guidelines

Ke Dang, Tuo Wang, Chengcheng Li, Jijie Zhang, Shanshan Liu, and Jinlong Gong declare that they have no conflict of interest or financial conflicts to disclose.

Supplementary Information

http://engineering.org.cn/EN/10.1016/J.ENG.2017.03.005
Experimental section
Figs. S1–S13
Table S1
Refs. [1–7]

References

[1] Fujishima A, Honda K. Electrochemical photolysis of water at a semiconductor electrode. Nature 1972;238(5358):37–8.
[2] Nellist MR, Laskowski FAL, Lin F, Mills TJ, Boettcher SW. Semiconductor-electrocatalyst interfaces: Theory, experiment, and applications in photoelectrochemical water splitting. Acc Chem Res 2016;49(4):733–40.
[3] Gao M, Sheng W, Zhuang Z, Fang Q, Gu S, Jiang J, et al. Efficient water oxidation using nanostructured α-nickel-hydroxide as an electrocatalyst. J Am Chem Soc 2014;136(19):7077–84.
[4] Zhong DK, Cornuz M, Sivula K, Gratzel M, Gamelin DR. Photo-assisted electrodeposition of cobalt-phosphate (Co-Pi) catalyst on hematite photoanodes for solar water oxidation. Energy Environ Sci 2011;4(5):1759–64.
[5] Seabold JA, Choi KS. Effect of a cobalt-based oxygen evolution catalyst on the stability and the selectivity of photo-oxidation reactions of a WO_3 photoanode. Chem Mater 2011;23(5):1105–12.
[6] Dincă M, Surendranath Y, Nocera DG. Nickel-borate oxygen-evolving catalyst that functions under benign conditions. Proc Natl Acad Sci USA 2010;107(23):10337–41.
[7] Bediako DK, Lassalle-Kaiser B, Surendranath Y, Yano J, Yachandra VK, Nocera DG. Structure-activity correlations in a nickel-borate oxygen evolution catalyst. J Am Chem Soc 2012;134(15):6801–9.
[8] Choi SK, Choi W, Park H. Solar water oxidation using nickel-borate coupled $BiVO_4$ photoelectrodes. Phys Chem Chem Phys 2013;15(17):6499–507.
[9] Gan J, Lu X, Rajeeva BB, Menz R, Tong Y, Zheng Y. Efficient photoelectrochemical water oxidation over hydrogen-reduced nanoporous $BiVO_4$ with Ni-B_i electrocatalyst. ChemElectroChem 2015;2(9):1385–95.
[10] Zhang P, Wang T, Chang X, Zhang L, Gong J. Synergistic cocatalytic effect of carbon nanodots and Co_3O_4 nanoclusters for the photoelectrochemical water oxidation on hematite. Angew Chem Int Ed 2016;128(19):5945–9.
[11] Li C, Hisatomi T, Watanabe O, Nakabayashi M, Shibata N, Domen K, et al. Positive onset potential and stability of Cu_2O-based photocathodes in water splitting by atomic layer deposition of a Ga_2O_3 buffer layer. Energy Environ Sci 2015;8(5):1493–500.
[12] Berglund SP, Abdi FF, Bogdanoff P, Chemseddine A, Friedrich D, van de Krol R. Comprehensive evaluation of $CuBi_2O_4$ as a photocathode material for photoelectrochemical water splitting. Chem Mater 2016;28(12):4231–42.
[13] Kumagai H, Minegishi T, Sato N, Yamada T, Kubota J, Domen K. Efficient solar hydrogen production from neutral electrolytes using surface-modified Cu(In,Ga)Se_2 photocathodes. J Mater Chem A 2015;3(16):8300–7.
[14] Wang Z, Liu G, Ding C, Chen Z, Zhang F, Shi J, et al. Synergetic effect of conjugated $Ni(OH)_2/IrO_2$ cocatalyst on titanium-doped hematite photoanode for solar water splitting. J Phys Chem C 2015;119(34):19607–12.
[15] Kim JY, Youn DH, Kang K, Lee JS. Highly conformal deposition of an ultrathin FeOOH layer on a hematite nanostructure for efficient solar water splitting. Angew Chem 2016;128(36):11012–6.
[16] Ahmed AY, Ahmed MG, Kandiel TA. Modification of hematite photoanode with cobalt based oxygen evolution catalyst via bifunctional linker approach for efficient water splitting. J Phys Chem C 2016;120(41):23415–20.
[17] Malara F, Minguzzi A, Marelli M, Morandi S, Psaro R, Dal Santo V, et al. α-Fe_2O_3/NiOOH: An effective heterostructure for photoelectrochemical water oxidation. ACS Catal 2015;5(9):5292–300.
[18] Klahr B, Hamann T. Water oxidation on hematite photoelectrodes: Insight into the nature of surface states through *in situ* spectroelectrochemistry. J Phys Chem C 2014;118(19):10393–9.
[19] Yatom N, Neufeld O, Toroker MC. Toward settling the debate on the role of Fe_2O_3 surface states for water splitting. J Phys Chem C 2015;119(44):24789–95.
[20] Le Formal F, Tetreault N, Cornuz M, Moehl T, Gratzel M, Sivula K. Passivating surface states on water splitting hematite photoanodes with alumina overlayers. Chem Sci 2011;2(4):737–43.
[21] Du C, Yang X, Mayer MT, Hoyt H, Xie J, McMahon G, et al. Hematite-based water splitting with low turn-on voltages. Angew Chem Int Ed 2013;52(48):12692–5.
[22] Kim TW, Choi KS. Nanoporous $BiVO_4$ photoanodes with dual-layer oxygen evolution catalysts for solar water splitting. Science 2014;343(6174):990–4.
[23] Luo Z, Li C, Liu S, Wang T, Gong J. Gradient doping of phosphorus in Fe_2O_3 nanoarray photoanodes for enhanced charge separation. Chem Sci 2016;2017(8):91–100.
[24] Chang X, Wang T, Zhang P, Zhang J, Li A, Gong J. Enhanced surface reaction kinetics and charge separation of p-n heterojunction $Co_3O_4/BiVO_4$ photoanodes. J Am Chem Soc 2015;137(26):8356–9.
[25] Xu Y, Wang X, Chen H, Kuang D, Su C. Toward high performance photoelectrochemical water oxidation: Combined effects of ultrafine cobalt iron oxide nanoparticle. Adv Funct Mater 2016;26(24):4414–21.
[26] Zhang M, Luo W, Zhang N, Li Z, Yu T, Zou Z. A facile strategy to passivate surface states on the undoped hematite photoanode for water splitting. Electrochem Commun 2012;23:41–3.
[27] Han L, Dong S, Wang E. Transition-metal (co, Ni, and Fe)-based electrocatalysts for the water oxidation reaction. Adv Mater 2016;28(42):9266–91.
[28] Ye KH, Wang Z, Gu J, Xiao S, Yuan Y, Zhu Y, et al. Carbon quantum dots as a visible light sensitizer to significantly increase the solar water splitting performance of bismuth vanadate photoanodes. Energy Environ Sci 2017;10(3):772–9.
[29] Trześniewski BJ, Diaz-Morales O, Vermaas DA, Longo A, Bras W, Koper MTM, et al. *In situ* observation of active oxygen species in Fe-containing Ni-based oxygen evolution catalysts: The effect of pH on electrochemical activity. J Am Chem Soc 2015;137(48):15112–21.
[30] Dionigi F, Strasser P. NiFe-based (oxy)hydroxide catalysts for oxygen evolution reaction in non-acidic electrolytes. Adv Energy Mater 2016;6(23):1600621–40.
[31] Pham HH, Cheng MJ, Frei H, Wang LW. Surface proton hopping and fast-kinetics pathway of water oxidation on Co_3O_4 (001) surface. ACS Catal 2016;6(8):5610–7.
[32] Friebel D, Louie MW, Bajdich M, Sanwald KE, Cai Y, Wise AM, et al. Identification of highly active Fe sites in (Ni,Fe)OOH for electrocatalytic water splitting. J Am Chem Soc 2015;137(3):1305–13.
[33] Koper MTM. Theory of the transition from sequential to concerted electrochemical proton-electron transfer. Phys Chem Chem Phys 2013;15(5):1399–407.